

3D Atmospheric Tomography using UAVs

Kevin Rogers & Anthony Finn
Defence and Systems Institute,
University of South Australia,
Mawson Lakes, SA 5095, Australia

ABSTRACT

This paper presents a method for tomographically reconstructing spatially varying three-dimensional atmospheric temperature profiles and wind velocity fields based on measurements of the acoustic Doppler shift between a small Unmanned Aerial Vehicle (UAV) and ground-based microphones. The frequency measurements are used to estimate the acoustic propagation time between the UAV and the ground microphones, which in turn are affected by the atmospheric temperature and wind speed vectors along each sound ray path. The parametric fields are modelled as the weighted sum of Radial Basis Functions (RBFs), which also allow local meteorological measurements made at the UAV and ground receivers to supplement any Doppler Shift observations. The 3D tomographic technique has already been demonstrated using simulation. This paper summarises the tomographic technique and reports on the results from initial field trials. The technique has practical applications such as atmospheric research, boundary layer meteorology, air pollution measurements, analysis of wind shear, and wind farm surveys.

INTRODUCTION

The approach described in this paper makes use of techniques previously described in Finn & Franklin, 2011a Rogers & Finn, 2013a, 2013b. The techniques parasitically exploit the acoustic signature of a propeller-driven UAV, which consists of harmonic tones superimposed onto a broadband random component (Ferguson & Lo, 2000, Finn & Franklin 2011b). The narrowband signals are generated by the engine-firing sequence and propeller blade rate of the aircraft in flight; the broadband components of the signal are the result of airflow over microphones (which are onboard the UAV), mechanical vibration of the microphones, and electrical noise in the microphone pre-amplifiers. This paper presents a preliminary examination of data taken during some field trials.

The Doppler-shifted frequency of the narrowband tones received by the ground microphones are compared against the signature emitted by (and measured onboard) the UAV to determine the acoustic propagation delay of the relevant signal (Finn & Franklin, 2011a). From the range and range-rate information pertinent to the geometry, acoustic propagation latency data may be determined (Ferguson & Lo, 2007). Tomographic techniques may then be used to reconstruct 2D cross-sections or 3D atmospheric volumes of temperature profiles and wind velocity vectors (Rogers & Finn, 2013a). Computation of the atmospheric profiles may take place in real time if the source spectrum recorded onboard the UAV is accurately time-stamped together with the UAV's navigation data and transmitted to the ground using a radio link. These tones may be detected and tracked at ranges of up to 3km if the signal-to-noise ratio (SNR) is maximised appropriately (Finn & Franklin 2011b), although the ranges demonstrated in this trial extend only to about 1km.

This measurement technique offers a number of potential advantages over current techniques for observing meteorological parameters. The first is cost. Conventional approaches (e.g. SODAR, LIDAR or mast-mounted anemometers) require expensive hardware. In particular, the erection and maintenance costs of masts become very high as observation altitudes increase. This is not an issue for our technique, which – aside from the capital cost of the UAV – relies upon

hardware costing only a few thousand dollars. Secondly, the presence of masts, which are required for anemometry, can obstruct or distort local wind flow patterns (Wilson & Thomson, 1994). The technique described here does not introduce any obstructions that can distort such measurements; and it offers a $1/r^2$ range advantage over the two-way ($1/r^4$) propagation demands of SODAR techniques.

Thirdly, one of the main issues for existing outdoor acoustic tomography is the formulation of robust and accurate reconstructions of the temperature and wind-velocity fields from a spatially limited set of observations (Jovanovic, et al, 2009, Ostashev et al, 2008). In our approach, this is overcome as the resolution of the reconstruction of the atmospheric profiles is governed predominantly by the number and spacing of ground microphones and the duration of the observed spectra relative to the sampling regime (Rogers & Finn 2013a). The trajectories described by the UAV are also under user-control so the ray paths are controllable. This offers observational mobility and means that the size, shape and location of the measurement space can be easily modified 'on the fly'.

Fourthly, as the aircraft has no pilot, it can be made small, can travel slowly and therefore has low kinetic energy, which reduces the consequences of a crash. Thus, the UAV may be flown with relative safety at any altitude from a few metres to several kilometres, in dangerous environments, over complex terrains, or over rough terrain. Tomographic profiles can also be reconstructed for different regions of the atmosphere: the surface layer, which extends a few metres above the ground (although a propeller-driven aircraft flying so close to the ground may well disturb the atmosphere under observation); the boundary layer, which extends up to heights of a few hundred metres; or – subject to the performance envelope of the UAV – even up to heights of several kilometres; and potentially between moving aircraft.

TRIALS RESULTS

Field trials were conducted at St Leonards, VIC using an Aerosonde UAV (www.aerosonde.com). A linear array of 5 microphones was placed over a 400m baseline 0.5m above flat grassy terrain. The UAV was flown over a path that

commenced at an altitude of 500m and progressively descended to an altitude of about 100m, circling at both the top and bottom of the trajectory. The total flight time took about 6 minutes. **Figure 1** (upper) shows both the microphone locations (blue asterisks) and the UAV locations at 1 sec intervals (green crosses). The ray path geometry for the observations is shown in **Figure 1** (lower).

The standard positioning service, coarse acquisition code GPS receivers provide absolute measurements of position of both the ground receivers and the UAV. This has 1σ accuracy of around ±10m in the horizontal plane at but is less accurate in the vertical plane. UAV height was therefore measured using both GPS and an altimeter based on barometric pressure, calibrated when the UAV was on the ground and typically accurate to around ±3m. The relative accuracy of observations is estimated to be around ±3m as code differential GPS (DGPS) techniques were employed. These could be improved by using real time kinematic carrier phase DGPS techniques, which are commercially available and offer accuracies around ±0.1m. The UAV’s autopilot, which uses GPS and an inertial navigation system, was used to derive the velocity of the UAV, which is accurate to ±0.1m/s. The UAV carries two sensors fitted below/aft the trailing edge of its wings, which measure atmospheric pressure (±1.5hPa), air temperature (±0.5°C), and relative humidity (±5%). Wind speed and direction can also be measured (±0.8m/s). The sampling rate was 0.2Hz, referenced to GPS position and time.

The dominant features in the acoustic spectrum of a propeller-driven aircraft are the spectral lines corresponding to the engine firing sequence and propeller blade rate, which is equal to the propeller shaft rotation rate and the number of blades on the propeller. The propeller of the UAV has 2 blades and its engine rotated at about 5,800rpm (nominally 100Hz). It is driven by a 4-stroke engine whose cylinders fire every 2nd rotation, i.e. at approximately 50 Hz. Each of these sources also generates its own set of harmonics so there are a rich set of useful signals usually up to the 10th harmonic. These harmonics are linearly related so they all contain useful information for estimating the fundamental frequency (Rogers & Finn 2013a). The amplitude and frequency of the various harmonics vary over time as the engine load and hence firing sequence varies. **Figure 2** shows the UAV acoustic signal transmitted over the duration of the 360 sec trial. This is significantly more variable than typically experienced during other UAV flight trials. The reasons for this are not entirely clear, but are thought to be operator related.

To collect the data onboard the UAV a PCB-130A-40 ¼ inch ICP array free field low-profile surface pressure 45mV/Pa microphone with integral pre-amplifiers and a 24-bit, 102dB Spurious Free Dynamic Range (SFDR) is used in conjunction with a National Instruments NI-9234 USB Data Acquisition (DAQ) module. The sampling rate was 12.8 kHz (buffering problems prevented use of higher sampling frequencies). The ground receivers were Behringer ECM800 10mV/Pa condenser microphones that were sampled at 44.1 kHz using a 24 bit DAQ with 107dB SFDR.

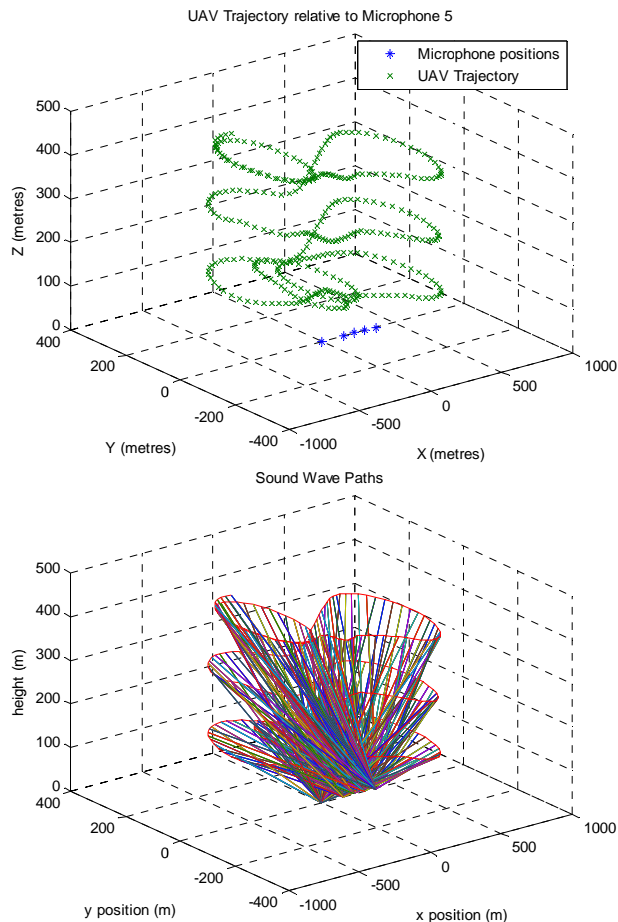


Figure 1: UAV flight trajectory and ground microphone locations (upper) and ray path geometry between UAV and ground microphones (lower)

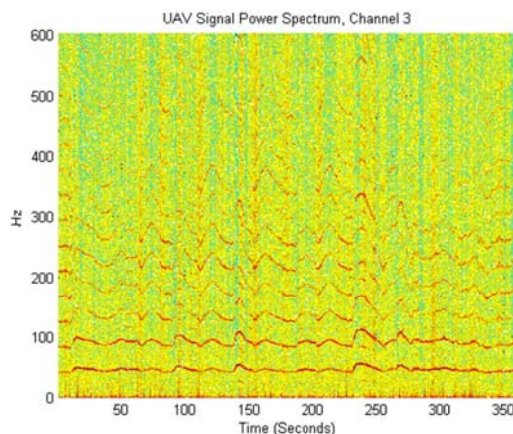


Figure 2: Spectrogram of acoustic signal emitted by the UAV over duration of trial

The effects of mechanical vibration on the UAV microphone were characterised and reduced through judicious selection of location and physical construction of the UAV. The effects of noise generated by airflow over the microphones (onboard the UAV) were reduced using small form-factor windshields and microphone mounts. As the trials were ‘piggybacked’ off others that required the microphones to be mounted externally to the UAV fuselage, a thin layer (2mm) of low density porous foam (8kg/m³) with a layer of synthetic fur covering the foam surface was used to reduce wind noise. This ad hoc

setup lowered flow noise by around 20dB. The absolute reduction in noise varies with frequency: high at lower frequencies and reducing as the frequency increases. The reduction at 15Hz is about 24dB but this drops to 12dB from 100 – 400Hz.

A time-frequency signal analysis of the UAV’s acoustic signature shows strong narrowband tones superimposed onto a broadband random component, with most of the narrowband energy below 2 kHz. The UAV data were processed in overlapping blocks, each containing 5 seconds of data, with 50% overlap between consecutive blocks. A 2^{16} point fast Fourier transform (FFT) with a Gaussian window was then used to compute the spectrum. The fundamental frequency was then estimated using the weighted sum of the first 10 harmonics. These harmonics were linearly related so they all contain useful information for estimating fundamental frequencies, $F_g(t)$ and $F_u(t)$, which represent the signals received at the ground and UAV microphones respectively.

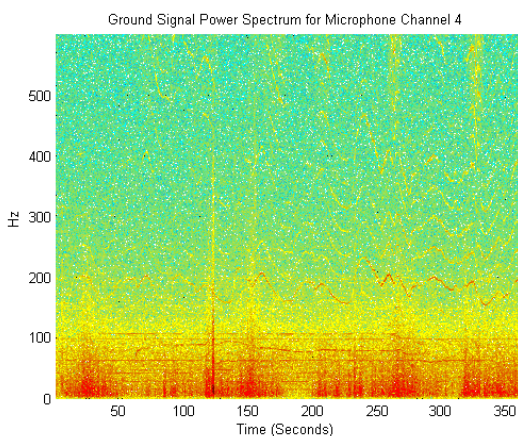


Figure 3: Spectrogram of signal received at a ground microphone. Dominant fourth harmonic is 180 ± 20 Hz

The signal to noise ratio of the signal received on the ground also varies with time due to variations in the signature emitted by the UAV (**Figure 3**), as well as atmospheric turbulence and wind flow noise over the microphones, which is greatest at low frequencies. Typically, multiple harmonics are visible (Lo & Ferguson, 2007, Finn & Franklin 2011b, 2012). Also clearly visible are spurious signals such as interferers, which show up as strong horizontal tones and tones not harmonically related to one another or the UAV engine firing sequence. These signals were excised during the front-end processing. The effects of wind noise on the ground microphones, which were inadvertently used without foam (i.e. wind noise) protection, are also clearly visible. This shows up as broad spectrum noise below 100 Hz and significantly reduces the SNR of several harmonics.

There is, however, one harmonic (the dominant fourth), clearly visible. This signal varies from 160 – 200 Hz and has sufficient SNR to allow propagation delays to be determined. The absence of the other harmonics, however, precludes use of the frequency estimation improvement techniques described in Rogers & Finn 2013b (except onboard the UAV).

Despite the poor SNR, it should also be noted that the fourth harmonic (~ 180 Hz ± 20 Hz) of the UAV is visible at the extremes of the flight path. That is, the current signal processing techniques easily detect the UAV at ranges of ~ 1 km thereby extending the range over which current atmospheric observations may be made, e.g. using equipment such as SODAR (and offering estimates of temperature profiles).

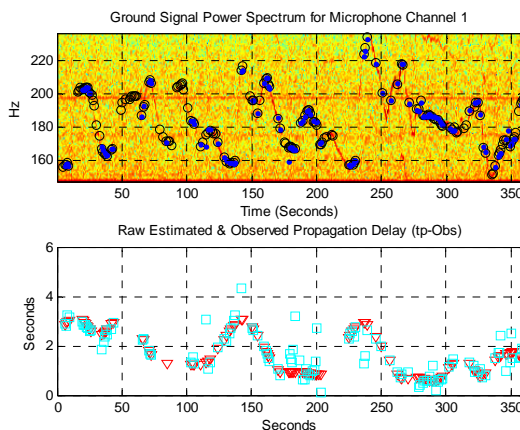


Figure 4: Measured frequency variations at a ground microphone (upper) and estimated propagation delay (lower).

The results of the processing are shown in **Figure 4**. The upper subplot shows the estimates of peak frequency for the fourth harmonic superimposed onto the (zoomed) spectrogram of **Figure 3** at each calculated arrival time, $t_i + \Delta t_{pi}$ where t_i are the emission epochs, i . The lower plot shows the nominal propagation delay, $\Delta t_p = l(t)/c_0$ (red triangles), where $l(t)$ is the distance between the UAV and the microphone and c_0 the nominal speed of sound, and the delay calculated using equation (5) (cyan squares) as a function of time. Only ray paths that have estimates of both F_u and F_g are used, where F_u and F_g are the transmitted and received frequencies. After outliers (any Δt_p that implies a speed of sound exceeding ± 35 m/s from nominal) have been removed and the data smoothed using a 15-point moving average, the average difference between nominal and observed propagation delays is 1-2ms for each microphone, with standard deviation of 10-20ms. This represents an average deviation from nominal of approximately 0.1% and 1σ variations of about 1%, i.e. up to two orders of magnitude higher than those used in the simulations of Rogers & Finn, 2013a, 2013b.

Despite the high levels of noise the UAV and ground microphone data were combined to determine the signal propagation delay. All Ray paths dissecting the intervening atmosphere are effectively treated as a 2D cross-section in the x-z plane rather than 3D volume. In other words, the rays were projected onto a vertical plane intersecting the ground microphone array along its length and the tomographic inversion carried out in 2D. Also, due to the high level of observational noise and the small number of microphones deployed only 4 RBF were used, providing only modest resolution of atmospheric scale size. These RBFs were spaced uniformly throughout the observation area (one in each quadrant) and all observations that do not fully intersect all four RBF discarded. After the filtering, approximately 100 useful observation equations remain. The RBF coefficients that represent the amplitudes of the temperature and wind velocity deviations from the nominal atmospheric conditions were then calculated using least squares (Rogers & Finn 2013a).

The results of this inversion are shown in **Figure 5**. The x-axis represents the line through the array of ground microphones, with microphones located at (roughly) 0m, 150m, 225m, 300m and 375 m. Temperature is colour coded, wind magnitude and direction are shown as series of small black arrows. The temperature is observed to fall from a peak of about 21.5°C (bottom left of the image) to a minimum of 17.5°C (top left of the image). This represents a fall of about

0.8°C per 100m, a figure typical of the adiabatic lapse rate. The thermodynamic temperature observed by the UAV is corrected for the addition of water vapour, i.e. it is converted to virtual acoustic temperature.

The wind vectors vary from 1.5m/s to 4.9m/s in the horizontal direction and 0.3m/s to 0.8m/s in the vertical direction. An estimate of the accuracy of these results may be obtained from the mean square error of the residuals of the RBF coefficients, 0.9°C, 4.4m/s and 1.3m/s for the temperature and x- and z-wind vectors, respectively.

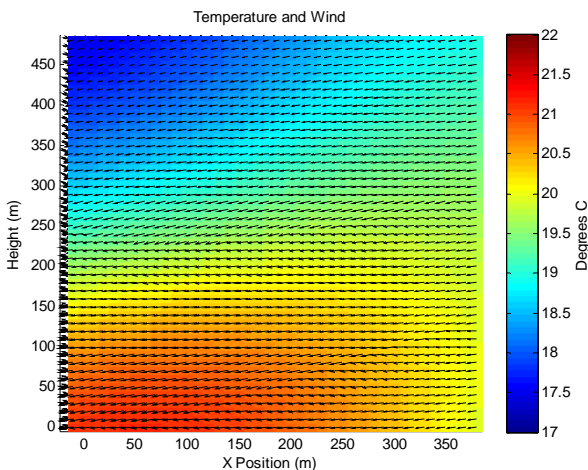


Figure 5: 2D temperature & wind velocity profiles derived using UAV-based acoustic tomography.

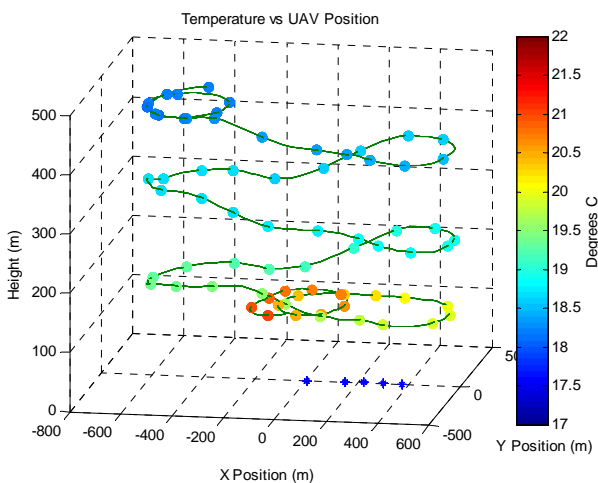


Figure 6: Temperature observations made by meteorological sensors onboard UAV as a function of Cartesian geometry

Although these residuals imply rather poor accuracy, the inversion results compare very favourably with the direct observations taken onboard the UAV (**Figure 6**). In particular, both horizontal and vertical gradients broadly conform. Wind vector observations have not been compared at this stage, but appear high, particularly in the Z-direction. The reasons for this are not yet understood.

It must be stressed that while the results of the inversion look plausible they are not yet validated. For reasons that are not yet entirely clear to the authors the estimates are sensitive to the effects of filtering: the general structure of the result remains largely unchanged (warm bottom left and cool top right, horizontal gradients as shown) but different filtering delivers differing absolute values of temperature and wind

velocity. This is thought to be a combination of inadequate treatment of the effects of noise in determination of the propagation delays and subsequent inversion, inadequate relaxation of nominal (i.e. background) temperature and wind velocities in the least squares adjustment also contributes, and other propagation effects that are yet to be accounted for in the modelling.

CONCLUDING REMARKS

Based on earlier published work the paper describes the outcome of some preliminary atmospheric tomography field trials for which plausible temperature and wind speed profiles have been obtained. At this early stage of our analysis, the trials results broadly accord with meteorological observations taken onboard the UAV and suggest real-world viability for the technique. The current signal processing limits the overall accuracy and spatial resolution of the technique, which is modest. However, unlike existing methods of meteorological observation estimates of temperature and wind vectors are obtained simultaneously.

At present the detection ranges have been limited to around 1km, but even this offers extended atmospheric observation over existing techniques such as SODAR, and a degree of mobility not available from LIDAR, radar, anemometry, SODAR, etc. Future work will focus on determining more accurate estimates of the propagation latency both through better estimation of the narrowband tones (both onboard the UAV and at the ground microphones) and through coding techniques described in Finn & Franklin 2011a). Application of techniques that exploit multiple harmonics, together with the examination of the relationship between the accuracy of the frequency estimation and the temporal and spatial resolution available from the techniques, are also a priority for the researchers; as are reducing wind noise on the ground microphones, improving the resolution available from the tomographic inversion, determining the overall performance envelope of the approach, extending observation ranges, and validating the results against other meteorological observations.

ACKNOWLEDGEMENTS

We are very grateful to our colleagues Stephen Franklin and Maurice Gonella of UniSA and Aersonde respectively, who conducted the flight trials at St Leonards.

REFERENCES

Ferguson, B.G. & K.W. Lo, 2000: Turbo-prop and rotary-wing aircraft flight parameter estimation using both narrow-band and broadband passive acoustic signal processing methods, *J. Acoustic Society America*, Vol. 108, No. 4.

Ferguson, B.G., K.W. Lo & R. Wyber, Acoustic sensing of direct and indirect weapon fire, *Proceedings Intelligent Sensor, Sensor Networks & Information Processing Conference 2007*, Melbourne, December 2007

Ferguson, B.G. & Quinn, Application of the short-time Fourier transform and the Wigner-ville distribution to the acoustic localisation of aircraft, *Journal of Acoustic Society of America*, Vol. 92, August 1994.

Finn, A. & S. Franklin, 2011a: UAV-Based Atmospheric Tomography, *Proc. Australian Acoustical Society Conference 2011*, Gold Coast, Australia, Nov 3-4.

Finn, A. & S. Franklin, 2011b: Acoustic Sense & Avoid for UAVs, *Proc. Intelligent Sensor Signal Network & Information Processing (ISSNIP) Conference*, Adelaide.

Finn, A. & S. Franklin, 2012: Trials results for Acoustic Sense & Avoid for UAVs, *Defence and Systems Institute*

- Report for AAI/Aerosonde, DA-AS-085-D0070, October 2012.
- Jovanovic, I., 2008: Inverse problem in acoustic tomography: Theory and applications, Ph.D. Thesis, Ecole Polytechnique Federale de Lausanne (EPFL), pp139.
- Jovanovic, I., et al, 2009: Acoustic tomography for scalar and vector fields: Theory and application to temperature and wind estimation, *J. Atmos. & Oceanic Technol.*, Volume 26, August, p1475-1492.
- Lo, K.W. & B.G. Ferguson, Tactical unmanned aerial vehicle localisation using ground-based acoustic sensors, *Proceedings Intelligent Sensor, Sensor Networks & Information Processing Conference 2004*, Melbourne, December 2004
- Ostashev, V.E., *Acoustics in a moving inhomogeneous medium*, Thompson, ISBN-0-419-22430-0, 1997
- Ostashev, V.E., A.G. Voronovich & D.K. Wilson, *Acoustic tomography of the atmosphere*, *Proc. IEEE International Geoscience & Remote Sensing Symposium*, 2000
- Ostashev, V.E., et al, 2008: Recent progress in acoustic tomography of the atmosphere, *Proc. 14th International Symposium for the Advancement of Boundary Layer Remote Sensing*, IOP Conference Series (Earth & Environmental Science) IOP Publishing.
- Rogers K. & A. Finn, Three-dimensional atmospheric tomography using UAVs, *Journal of Atmospheric & Oceanic Technology*, Vol. 30, Issue 2, Issue 2, 336-344, February 2013
- Rogers K. & A. Finn, Frequency estimation for 3D UAV-based atmospheric tomography, Submitted, *Proceedings of IEEE International Conference on Intelligent Sensors, Sensor Networks and Information Processing (ISSNIP)*, April 2013
- Wiens, T. and P. Behrens, 2009: Turbulent flow sensing using acoustic tomography, *Proceedings of Innovations in practical Noise Control 2009*, Ottawa, Canada.
- Wilson, D. K., and D. W. Thomson, 1994: Acoustic tomographic monitoring of the atmospheric surface layer, *J. Atmos. Oceanic Technol.*, 11, p751–769.
- Wyber, R., UAV Acoustic Collision Avoidance, private communication, July 2012
- Ziemann, K. Arnold, & A. Raabe, Acoustic travel time tomography—A method for remote sensing of the atmospheric surface layer, *Meteorological Atmospheric Physics*, 71, p43–51, 1999